Thermophysics and Aeromechanics, *2020*, *Vol. 27*, *No. 4*

DOI: 10.1134/S0869864320040101

Processes of fuel self-ignition and flame stabilization with transverse hydrogen fuel injection into a supersonic combustion chamber*

M.A. Goldfeld

Khristianovich Institute of Theoretical and Applied Mechanics SB RAS, *Novosibirsk*, *Russia*

E-mail: gold@itam.nsc.ru

(*Received November 18*, *2019*; *revised March 24*, *2020*; *accepted for publication April 28*, *2020*)

The paper presents a study for conditions for hydrogen self-ignition and flame spreading in a supersonic combustion chamber at the Mach number for the inlet flow equal to 4. The experimental model is a rectangular channel with a flame stabilizer performed as a backward-facing step. The fuel was injected before the step at the top and bottom walls through 8 round orifices which were oriented at angles 45° or 90°. Testing was performed for a wide range of flow parameters which were close to the flight conditions. The experiments performed allowed an efficient scheme of fuel injection for the processes of self-ignition and flame stabilization, which permits preventing choking the channel. It was found that the choice of the injection scheme and fuel injection pressure are critical for ignition conditions and allow controlling the combustion process.

Keywords: supersonic flow, ignition, combustion, flame stabilization, flow control.

Introduction

Fuel ignition and flame stabilization for combustion of gaseous or liquid fuel in airflow is one of fundamental problems in physics of combustion: this problem can be solved at the interface of aerodynamics, thermodynamics, and chemical kinetics. During several last decades, a multitude of complex processes were studied that related to the processes of ignition and combustion of different types of fuel. In recent years, numerous efforts have been allocated to the study of combustion and appropriate conditions in supersonic flows in a combustion chamber. This new direction of research was initiated by a need in developing hypersonic flight vehicles with a hypersonic air-breathing jet engine (scramjet). Recent studies in engineering of a hypersonic vehicle with scramjet demonstrated technical feasibility and economic efficiency of using the hypersonic transportation system, including the systems for cargo delivery to the orbit [1, 2].

* The research was carried out within the framework of the Program of Fundamental Scientific Research of the state academies of sciences in 2013–2020 (Project No. AAAA-A17-117030610126-4). The study was conducted at the Joint Access Center «Mechanics» of ITAM SB RAS.

A characteristic feature of scramjet is the supersonic velocity for the flow at the combustion chamber inlet [3]. When the vehicle flight speed increases up to Mach 8–12, the speed at the channel inlet corresponds to the range of Mach number from 2.5 to 4. At this flow velocity, the fuel (or fuel mixture) time of residence in the combustion chamber is very low (~ 1 ms). In combination with rather low static pressure (~ 0.05 MPa), this derives complications for mixing, ignition, and stability conditions for reliable combustion [4, 5]. Therefore, achieving of effective ignition and stable combustion in a high-speed stream remains a serious problem in designing of scramjet engines, for which the solution requires a comprehensive approach [6].

Different gas-dynamic and designing approaches were used to ensure flame ignition and flame stabilization: backward-facing step [7, 8], cavity [9–11], different kinds of struts [12, 13] and combinations of those approaches [14 –16]. However, the listed approaches not always ensure self-ignition of the fuel mixture at high temperatures of flow. In particular, the studies found that using of a cavity as a flame stabilizer cannot provide effective combustion even at moderate supersonic velocities at the combustion chamber inlet ($M_{inl} = 2$). Therefore, the struts are needed for additional deceleration of flow and for fuel injection into the flow core [14]. The angle-oriented hydrogen injectors within the combustion chamber with a backward-facing step also failed to ensure efficient mixing and intensive burning [15]. The reason for this result is a failure to arrange the interaction between the separation zones behind the step (in a cavity) with the stream core that reduces the mixing efficiency. The main disadvantage of using struts in the combustion chamber is the growth of drag force and unreliable positive outcome [11, 15], especially for a higher inlet flow velocity. That is why different methods of artificial ignition have been used: a pilot flame, discharges, and plasma-triggered ignition [17, 18]. However, these methods produce a high-pressure loss and significant complication in the combustion chamber construction [17, 19], which requires additional energy sources for ignition.

Analysis of prior art in the field of flame ignition and stabilization revealed that the most studies have been focused on testing the combustion chambers with the inlet Mach number 1.5–2.5 and the use of intrusive methods for fuel injection (struts, wedge-like injectors, vortex devices). The jet-like fuel injection on the walls was used less often and not quite successfully. We can speculate about two reasons for this. Usually, this class of research dealt with one-wall fuel injection because of combustion chamber design. These studies were restricted by a low fuel excess factor [20] and, as consequence, a low pressure of fuel injection and smallish jet penetration depth). This approach cannot solve the problem of balanced injection of fuel to the near-wall zone of combustion chamber where ignition begins and into the flow core for better efficiency of mixing and combustion [21]. However, the previous studies on penetration and mixing of counter hydrogen jets demonstrated that the flow structure enables fuel supply to the recirculation zones (zones for self-ignition) and to the flow core (for combustion). It was found that jet penetration and mixing efficiency can be regulated through the control of fuel injection pressure [22]. This result is achieved through counter injection of fuel into the channel and through jet interaction.

Although this field has many numerical simulation studies [23–26], we still lack a reliable and comprehensive theory that would explain the mechanisms of flame stabilization using flame stabilizers with different geometries, which needed to generate the recirculation flows. Therefore, the researchers use approximate methods in computations for the combustion method based on available experimental data [27–29]. Presently, experimental data are crucial for computation and analysis of processes in the combustion chamber of a scramjet. Obtaining and generalization of data on the basis of theoretical assumptions is the most effective approach for the development and verification of methods for calculation of a combustion chamber [26, 28].

Regardless of big efforts for studying the flame ignition and stabilization in the case of supersonic flow, the key physical and chemical mechanisms, features of ignition, flame spreading, and heat release in combustion chamber remain scarcely studied [2, 6, 30]. Available experimental studies and mathematical modeling are somewhat scattered and have unsystematic character. Therefore, it is difficult to evaluate the compliance of results obtained for different

methods of flame stabilization, different kinds of fuel, and problems with different thermodynamic parameters, typically, numerous. A huge amount of combinations of input parameters and limited financing make this task hard-to-solve [31].

From the technology point of view, it can be concluded that flame self-ignition and stabilization is a key aspect in engineering of a scramjet. The flame stabilization with a minimal value of pressure loss and high heat release is crucial for the engine with a high performance.

The purpose of this paper is the study of conditions and mechanisms for hydrogen self-ignition in a supersonic flow with the Mach number at the combustion chamber inlet equal to 4 without any intrusive device or artificial ignition. The main task is a study of how the angle of hydrogen injection influences the fact of ignition and flame stabilization. The main task consists in study the influence of the angle of hydrogen supply on the implementation of ignition and stable combustion, research of the ability to control the combustion process and prevent choking the channel (if any) by choosing the fuel supply scheme, and the pressure increase dependence in the combustion chamber and choking the channel on the fuel-air equivalent ratio.

1. Experimental setup and the model of combustion chamber

The study of operating supersonic combustion chamber was performed in a regime of attached pipeline (Fig. 1). This allows using a hotshot wind tunnel as a source of high-enthalpy working gas (air) [32]. This setup is an effective tool for that kind of study since provides the tests under the conditions close to the flight conditions. This setup provides not only required inlet Mach number, but also the proper pressure and temperature at the combustion chamber inlet for the entire range of stream velocity. Since the temperature strength of the tested model does not create any technology problems, the tests can be carried out under the conditions close to the flight conditions. Besides, the bigger sizes of the combustion chamber extend the opportunities in diagnostics of flow/flame and using a modular approach in assembly of the combustion chamber for a wider range in parametric study.

The experimental model of combustion chamber is a rectangular channel; it comprises the isolator section and the combustion chamber with the cross section 100×100 mm (Fig. 2). A flame stabilizer as a backward-faced step with the height of 25 mm is installed at the channel inlet. Downstream this stabilizer, we have a constant cross-section zone and next to it a diverging zone with the total opening angle of 12°. The initial value of air pressure in the discharge chamber of the wind tunnel and condensers voltage provide the proper pressure and temperature of the flow. Application of the second (throttling) prechamber allowed getting the proper pressure at the model inlet. The isolator section with the channel cross section of 50×100 mm and a unit of sonic injectors were unchanged during the tests. The calibration tests confirmed that the Mach number was stable during testing and the inlet flow is uniform [33]. Optical windows were allocated over the channel length for flow visualization and identification of flame propagation in the channel. The fuel injection is carried out through eight uniformly allocated holes oriented at the angle 45° or 90°. The fuel injectors are installed in front of the stabilizer at the top and bottom walls of the combustion chamber. The fuel injection system has the fuel tanks, supply pipelines, closure valves, and a synchronization system.

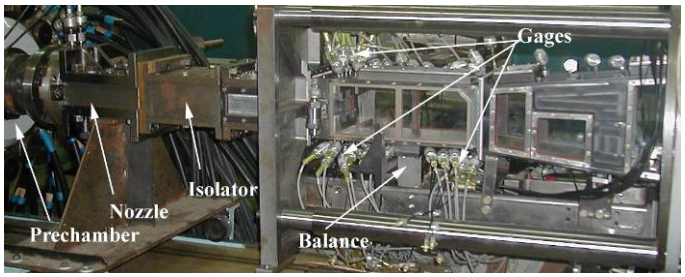

Fig. 1. Model of combustion chamber.

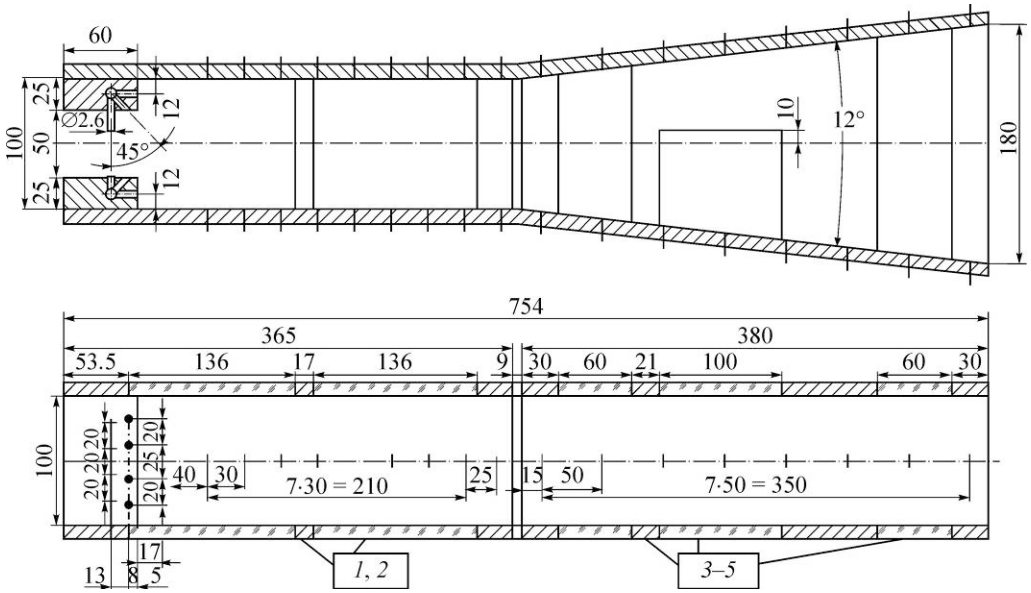

Fig. 2. Diagram of the combustion chamber model.
Sizes are given in mm; *1–5* — optical windows allocated over the channel length.

The model was tested under the following inlet conditions: Mach number $M_{inl} = 4$, the total temperature T_t was in the range from 1500 to 2400 K, static pressure from 0.06 to 0.25 MPa. The fuel-air equivalence ratio can be varied from 0.25 to 1.2. Experiments were carried out at different jet-to-crossflow momentum flux ratios — $J = (\rho V^2)_j / (\rho V^2)_0$, which were varied from 1.6 to 9.8. Here ρ and V are the flow density and velocity, and superscripts j and 0 indicate the jet and the main cross flow. The parameter J is very important for defining the jet penetration into the crossflow [34] and it is critical for jet characteristics and the flow structure in the channel [22, 35].

Feature of hotshot wind tunnel is a decrease of flow parameters during the operation regime (120–150 ms). Meanwhile, the value of fuel-air equivalence ratio (β) was kept constant during the entire experiment. The following parameters were measured during tests: the total gas pressure in the first and second prechambers of IT-302M wind tunnel; distribution of static pressure and heat flux in the channel, the base pressure near the step. The fuel-air ratio is calculated from measured pressure, temperature, and mass flow rates for hydrogen and air. The shadow visualization of flow and flame visualization in the visible spectra were performed. The setup has many points of measurement (more than 100) that permitted to obtain a detailed profile of static pressure and heat flux, including the value for base pressure and pressure in across directions.

2. Results and discussion

Previous studies [15, 33] demonstrated that in a flow with Mach number higher than 3, a reliable ignition and flame spreading over the entire volume of combustion chamber becomes problematic. It was demonstrated that flame initiation behind a step does not occur and combustion takes place only locally in the zones of interaction between shock waves and boundary layer, where the temperature of mixture and fuel-air composition are proper for combustion. Analysis of flow structure demonstrated that reliable ignition can be ensured through the formation of a separation zone with the size sufficient for mixture ignition. To achieve this goal, the wedges or struts are installed for stronger flow compression and reduction of flow velocity [16]. This initiates additional flow deceleration and a recirculation zone develops downstream

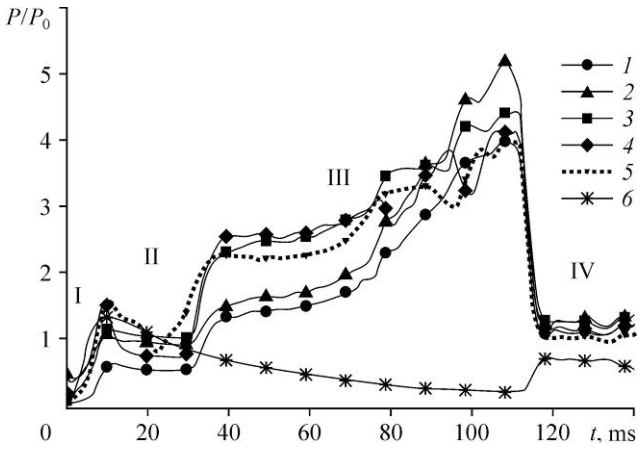

Fig. 3. Map of combustion stages in a supersonic combustion chamber for 45-degree fuel injection. $\beta = 0.95$; $X = 15$ mm (*1*), 85 mm (*2*), 175 mm (*3*), 235 mm (*4*), 295 mm (*5*), *6* — static pressure in the isolator section.

the stabilizer thus insuring a steady ignition mode [14, 15]. In this research, the generators of separation zones are the shock waves formed ahead of the fuel jets before the step [22, 34]. The shock wave inclination and intensity depend on the positions of fuel jets, jet angle, and fuel injection pressure. After analysis of numerous experimental data, the injection scheme (injectors allocation and diameter), pressure and angles for fuel injection was chosen.

The performed measurements found that when the fuel jets are supplied at the angle of 45°, the ignition starts at the distance of about 295 mm from the step, i.e., at the distance of (10–11) h, where h is the step height. This result is confirmed by pressure measurements (Fig. 3). Herein the relative pressure is a ratio of the static pressure in the combustion chamber to the static pressure in the isolator section in the front part of combustion chamber inlet. Obviously, this pressure starts increasing at the channel end with a constant cross section ($X = 295$ mm, line 5), and then the pressure wave spreads upstream. This result is in compliance with shadow visualization data (Fig. 4). This image demonstrates how the flame moves upstream toward the recirculation zone behind the step. The stages of ignition and flame spreading are indicated in Fig. 3. The ignition process occurs in three stages. Stage I corresponds to a local flame with moderate growth in pressure. The stage duration might vary from 6 to 30 ms, depending on the initial conditions of testing. This stage is characterized by flame spreading along the boundary layer both downstream and upstream from the initial ignition zone (Fig. 4). The image shows a thickening of near-wall layer with combustion and shows a high vorticity layer above this layer. Flow visualization confirms the fast spreading of flame upstream to the recirculation zone behind the step; this process is different for the top and bottom walls.

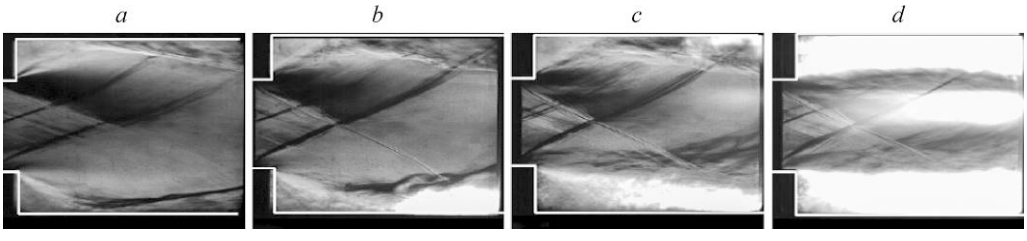

Fig. 4. Shadow visualization of flame propagation in the time interval between 5 ms and 10 ms. Herein the flow is directed from left to right; empty lines depict the contours of the upper and lower walls; time points: 5.5 ms (*a*), 6 ms (*b*), 7 ms (*c*), and 7.5 ms (*d*).

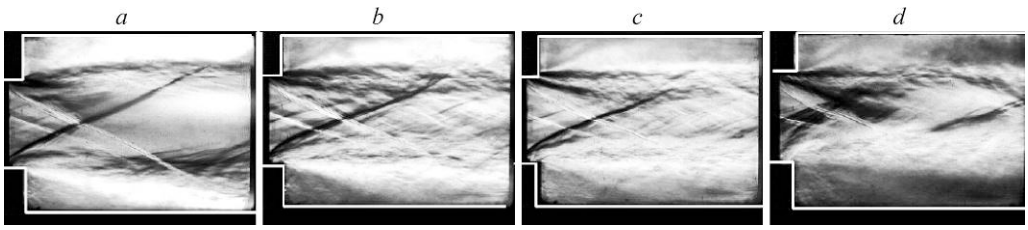

Fig. 5. Shadow visualization of flame propagation in the time interval of 20–90 ms.
$\beta = 0.95$; time points: 20 ms (*a*), 38 ms (*b*), 60 ms (*c*), and 86 ms (*d*).

Stage II (within the time interval from 20 to 90 ms) corresponds to intensive combustion and a higher pressure for the entire combustion chamber due to flame spreading in both directions through the mixing layer above the boundary layer (Fig. 5). The near wall layer becomes thicker and its thickness exceeds the boundary layer thickness and even the step height (Fig. 5*c*). As a result, the fuel jets and the mixing layer drift towards the stream core (and this increases the pressure in the channel). Meanwhile, the flow in the middle zone of channel remains a supersonic flow. The growth of heat release and, therefore, flow turbulization are followed by intensification of mixing and further spreading of flame through the combustion chamber. These processes go along with the expansion of near-wall zone of intensive combustion and by squeezing of the supersonic core (Fig. 5*d*) and by pressure growth in the channel.

Stage III (time interval between 90 and 135 ms) is characterized by steady combustion and the high level of pressure in the entire combustion chamber. Besides, the supersonic flow mode is retained in the flow core. The shadow images of flow in Figs. 6*a*–6*c* demonstrate the changes in the flow structure inside the combustion chamber while intense combustion that has reached the area up to the step. The supersonic zone in the flow core becomes much smaller and the supersonic flow retains mainly near the combustion chamber inlet (Fig. 6*b*). The shadow photographs demonstrate that the high-intensity turbulent layers in the subsonic zone of combustion near the walls become thicker. However, they do not merge within the distance of about 80–100 mm downstream the inlet cross section (Fig. 6*b*). The flame becomes more intense by the end of this zone that is confirmed by a stronger flame glow in the left part of the images in Figs. 6*b*–6*d*. Stage III goes before the channel choking and transition to the subsonic combustion: the latter begins at the 112th millisecond (see Fig. 3). This event is manifested in a drastic fall of the relative pressure in the channel that is caused by four-fold growth of the base pressure in the isolator section before the combustion chamber inlet in consequence of channel choking and increase of the pressure in the isolator ahead of the step.

Stage IV corresponds to combustion intensification and increase in heat release in the combustion chamber for the subsonic flow mode. This reduces the core of supersonic flow until its complete disappearance and channel choking while transition to the completely subsonic combustion. The shadow visualization at this stage is depicted in Fig. 6*d*. The overall flow zone behind the step is characterized by a subsonic flow without shock waves. The intense combustion zone shifts upstream and the flame occupies the most area of channel behind the step. This transition is preceded by a fast growth of the bottom pressure. The total pressure

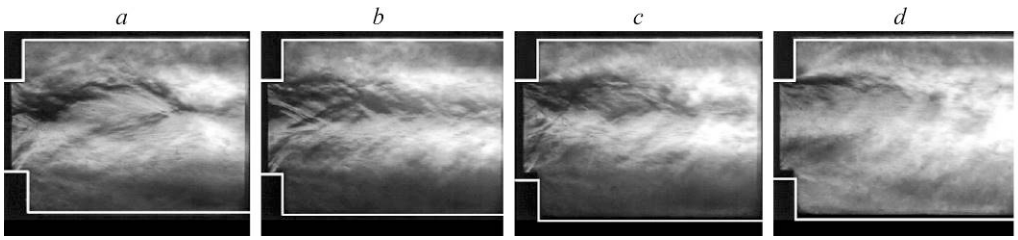

Fig. 6. Shadow visualization of flame propagation in the time interval of 90–135 ms.
$\beta = 0.95$; time points: 95 ms (*a*), 106 ms (*b*), 113 ms (*c*), and 134 ms (*d*).

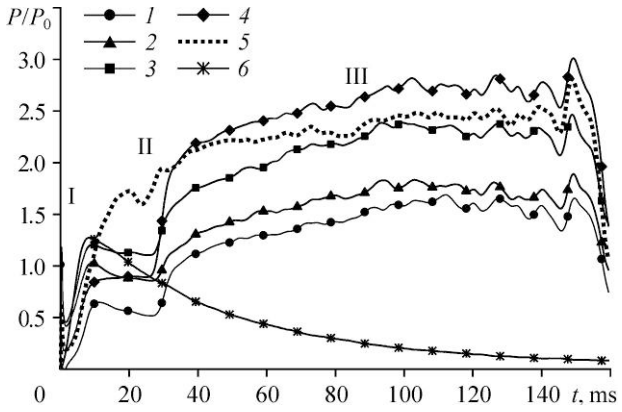

Fig. 7. Stages of combustion in the supersonic combustion chamber with fuel injection at 45 degrees.
$\beta = 0.67$; $X = 15$ mm (*1*), 85 mm (*2*), 145 mm (*3*), 205 mm (*4*), 295 mm (*5*), *6* — static pressure in the isolator section.

increases by factor of four not only within the combustion chamber, but also in the isolator section ahead the step (curve *1* in Fig. 3). This combustion mode is characterized by the growth of pressure pulsations and high turbulence.

To prevent the event of channel choking, the experiments at low fuel-air equivalence ratio ($\beta = 0.8$–0.5) were conducted. It was found that at $\beta = 0.67$, the channel choking and transition to subsonic combustion does not occur. Despite a significant reduction in pressure and temperature at the channel inlet during testing, the combustion continues until the end of setup operation. The time history of pressure under those conditions is plotted in Fig. 7. In contrast to the combustion process occurring at the fuel-air equivalence ratio $\beta = 0.95$, in the last case (at $\beta = 0.67$), only two regimes were realized in the combustion chamber: ignition stage II (time interval from the 5th to 30th millisecond) with a moderate pressure growth and stage III (from the 30th to 150th millisecond) characterized by intense combustion of hydrogen and the threefold increase in pressure. Note that the pressure during stage III corresponds to the maximum level during the second stage in our experiments with $\beta = 0.95$ (see Fig. 3). As it was previously, the ignition begins in the zone with coordinate $X = 295$ mm (see curve *5* in Fig. 7). The flame propagation pattern is the same as in the previous case, but the pressure and rate of flame propagation was lower (Figs. 8*a*–8*c*). The difference is the lack of pressure-growth stage similar to stage III (see Fig. 3). The pressure reaches the maximum value at time of 85 ms. It is close to the pressure in region II for the channel-choking regime (Fig. 3), but it does not spread upstream up to the isolator section (curve *6* in Fig. 7). The pressure in the base zone increased by less than twofold (curve *1* in Fig. 7) and remained steady until the end of combustion. This means that the combustor choking did not occur. Flow visualization in the combustion chamber for the case of steady combustion is presented in Fig. 8*d*. Obviously, here the supersonic flow

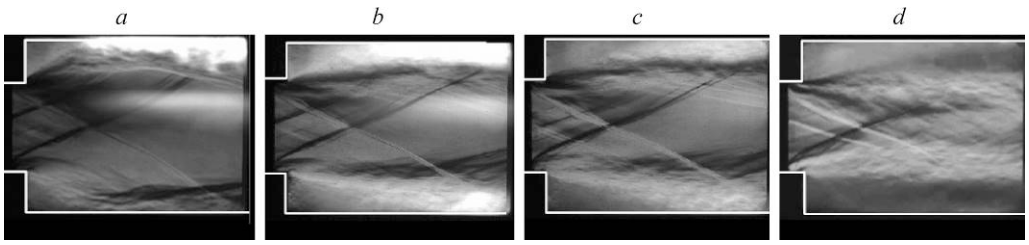

Fig. 8. Shadow visualization of flame propagation in the time interval of 7–106 ms.
$\beta = 0.67$; time points: 7 ms (*a*), 12 ms (*b*), 29 ms (*c*), and 106 ms (*d*).

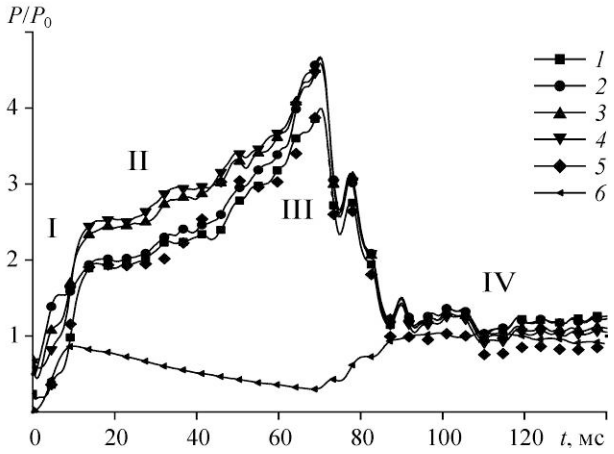

Fig. 9. Map of combustion stages in a supersonic combustion chamber with 90-degree fuel jet injection.
$\beta = 0.73$; $X = 15$ mm (*1*), 85 mm (*2*), 145 mm (*3*), 175 mm (*4*), 295 mm (*5*), *6* — static pressure in the isolator section.

mode sustains during the entire operation time. However, the supersonic core slightly decreases because of higher heat release due to the reduction of temperature at the combustion chamber inlet.

For the goal of evaluating the effect of fuel injection angle on fuel ignition and its combustion efficiency, experiments were conducted for fuel injection at the angle of 90°. It was found that for $\beta = 0.73$, all stages and properties of processes remain the same as at 45-degree fuel injection. However, the process of ignition and flame spreading occurs faster at a higher intensity. If the fuel was injected under the angle of 90°, a rapid simultaneous pressure growth was observed for entire channel, and the duration of stage I was less than 10 ms (Fig. 9). The ignition takes place at the distance of 110–140 mm from the step (curve *3* in Fig. 9), i.e., in the middle part of combustion chamber with a constant cross section. The pressure in this region was high during the whole combustion process. The pressure increase in the region II was much higher than for the case of fuel injection at the angle of 45°. This is due to more intense shock wave before the injected fuel jets and the size and position of separation zone occurring from interaction of the shock wave with the boundary layer downstream the step. This is the zone where mix ignition begins as shown in papers [15, 26]).

The shadow visualization of flow in the combustion chamber confirms the intensification of ignition for the case of fuel injection at 90-degres angle. The intensive combustion begins already on the 5th millisecond near the step (Fig. 10*a*). Visualization shows a rapid growth of the near wall layer and intense combustion in this region (8.5 ms). The intense turbulization of flow in the combustion zone and at the supersonic flow boundary facilitates the fast flame propagation and pressure growth in the combustion chamber. It gives pressure increase twice

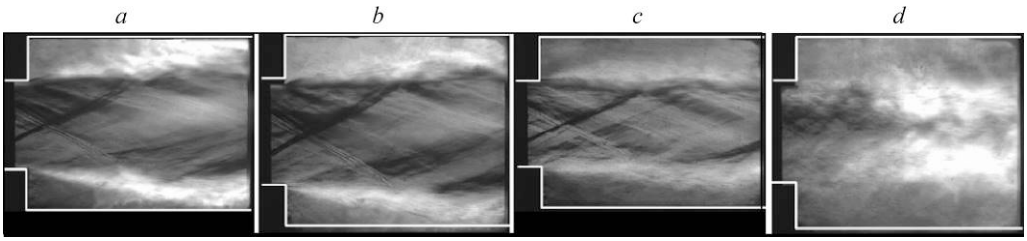

Fig. 10. Shadow visualization of flame propagation in the time interval of 5–72 ms.
$\beta = 0.73$; time points: 5 ms (*a*), 8.5 ms (*b*), 27.5 ms (*c*), and 70 ms (*d*).

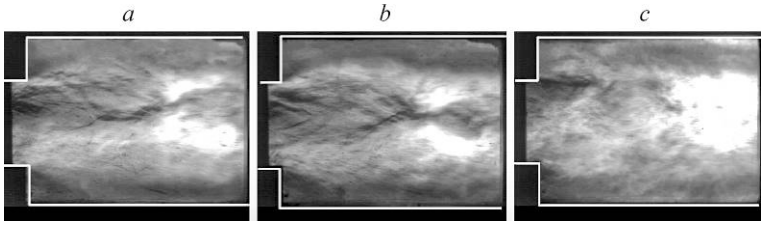

Fig. 11. Flow structure in the transition zone and choking zone for the time interval of 76–124 ms.
$\beta = 0.73$; time points: 76 ms (*a*), 84.5 ms (*b*), and 124 ms (*c*).

higher than for the configuration with 45-degree injection). Comparison of flow structure in photographs in Figs. 10*b* and 10*c* demonstrates that at higher heat release, the size of supersonic flow core decreases with a simultaneous pressure growth. This process completes with channel choking and transition to the subsonic combustion already at time of 70 ms (Fig. 10*d*).

Unlike the configuration with 45-degree of fuel injection, the transition from supersonic to subsonic mode of combustion at 90-degree fuel injection is longer and might take 10–20 ms. The static pressure during transition is characterized by high-amplitude low-frequency oscillations, as one can conclude from comparison of data shown in Figs. 3 and 9. The flow structure for the interval of transition (time range of 72–90 ms) and for the steady regime of choking (124 ms) is presented in Fig. 11. Obviously, the transition flow mode at the combustion chamber outlet retains a zone of supersonic flow. However, the size and structure of shock waves here vary in time (Figs. 11*a* and 11*b*), and this is a source of pressure oscillations.

Data comparison demonstrates that for both configurations, the mixture ignition occurs due to interaction between the shock wave and the boundary layer and the separation of the latter. The position of flame zone and intensity and the flame propagation velocity are defined by the size of separation zone and its proximity to the recirculation zone behind the step. For the configuration of 90-degree injection, choking the channel is inevitable even for the fuel-air ratio below 0.5. Meanwhile, the channel was not choked at this value of coefficient β when fuel was supplied at angle 45°. The reason is that the ignition zone was near the step and entire heat release occurs in a channel with a constant cross section. As a result, the flow in the channel reaches the sound speed, the pressure increases significantly and this pressure growth spreads upstream up to the isolator section. In this case, the diverging section has no influence on combustion and flow structure in the channel.

The evolution of pressure during the process of combustion chamber testifies that the increase in pressure correlates with the rate of heat flux. This conclusion is confirmed by experimental data shown in Fig. 12.

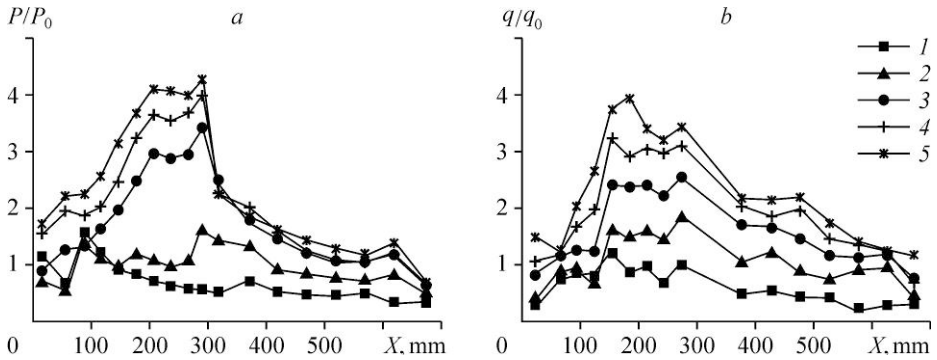

Fig. 12. Correlation between variation of pressure (*a*) and heat flux (*b*) for unsteady ignition of hydrogen fuel in the combustion chamber.
1 — 20 ms (no fuel injection), *2* — 10 ms, *3* — 20 ms, *4* — 30 ms, *5* — 40 ms.

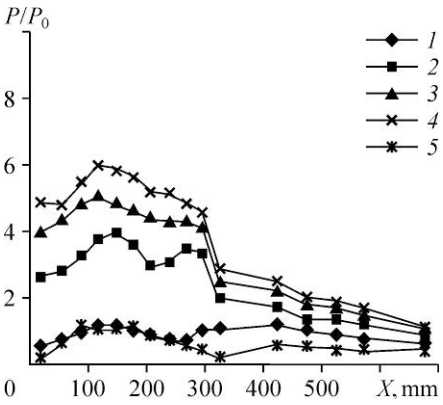

Fig. 13. Relative pressure in the channel at 45-degree fuel injection.
$\beta = 0.95$; *1* — 20 ms, *2* — 85 ms, *3* — 112 ms, *4* — 120 ms, *5* — 20 ms (no fuel injection).

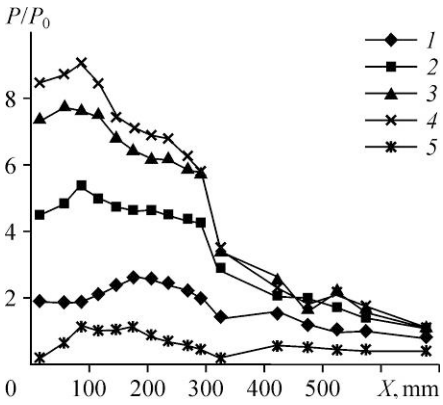

Fig. 14. Relative pressure in the channel at 90-degree fuel injection.
$\beta = 0.826$; *1* — 20 ms, *2* — 80 ms, *3* — 110 ms, *4* — 120 ms, *5* — 20 ms (no fuel injection).

Comparison of the laws of pressure and heat flux profiles variations along the channel length demonstrates their qualitative compliance, and even close quantitative similarity. Note that correlation between the pressure and heat flux is typical both of the steady combustion regime and of the unsteady mode of ignition (see the data in Fig. 12). This result confirms the option for identification of the intensity of combustion and heat release through the value of pressure growth over the combustion chamber length. This approach in evaluating the combustor characteristics through pressure is widely used in experiment and in numerical simulation studies [31, 36].

Comparison of pressure distribution along the channel length for different fuel injection angles demonstrates (Figs. 13 and 14) that the pressure inside the combustion chamber increases with the increasing fuel injection angle. The maximum pressure occurs at the injection angle 90° even at lower fuel-air equivalence ratio (β = 0.95 and 0.826 for Figs. 13 and 14, correspondingly). The change in the pressure peak position as a function of time depends on the fuel injection angle. For the variant of 90-degree fuel injection, the peak of maximal pressure drifts upstream and reaches a higher (about 1.5–1.7 times higher) level of pressure. The same proportion of pressures retains in the base area behind the step at X = 15 mm. Meanwhile, the intensity of combustion in the diverging section of the combustion chamber reduces due to the influence of expansion waves at the boundary between the sections during flow expansion at the entrance of the second section.

Comparison of flame glow intensity for two configurations of fuel injection is presented in Fig. 15. Flame visualization in the visible range confirms the existence of intense combustion in the front part of the combustion chamber with a constant cross-section area and 90-degree fuel injection (Fig. 15*a*). The images demonstrate propagation of flame for the entire cross

Fig. 15. Flame visualization for configurations with 90-degree (*a*) and 45-degree (*b*) fuel injection.

section up to the step. Comparison of flames for two different configurations demonstrates that the 90-degree configuration provides a higher intensity of combustion behind the step (as compared with configuration with jets injection at 45°). Figure 15*b* indicates that combustion at 45-degrees fuel injection occurs in initial part of combustor mainly near walls but not in the flow core. After-burning occurs at the channel end of the constant cross-section area at $X > 150$ mm and within the diverging part of the combustion chamber (windows number 3 and 4 in Fig. 2). This flame pattern is a result of changes in the efficient configuration of the channel and cross-section dimensions: this occurs due a change in position-and-size of the separation zones (mainly at the bottom zone behind the step). This enhances fuel-air mixing and reduces the effective length of combustion chamber where a complete fuel burnout takes place.

Conclusion

Testing of a supersonic combustion chamber model in a hot-shot setup performed under the test conditions, which are close to the flight ones, makes it possible to draw the following conclusions.

Combustion initiation occurs near the walls in the zones of the boundary layer separation induced by interaction between the reflected shock wave and the boundary layer if the proper proportions of fuel-air mixing are achieved. Exactly, this area is a source of flame initiation and the following flame spreading in upstream direction. The near-wall combustion is critical for flame stability and flame propagation over the whole channel up to the step. If the ignition energy is high enough, a wide subsonic zone is formed, which enables steady combustion in the supersonic flow core through the mixing layer.

The change in fuel injection angle can be an effective tool for control of ignition zone and combustion intensity. It is suitable method for avoiding the flow transition to the subsonic combustion and choking the channel.

The recirculation zone behind the step is not a source of ignition. The role of this zone is ensuring the flame stabilization and preventing disturbance spreading upstream (into the isolator section), which, in turn, excludes choking the channel.

This approach gives an opportunity to reduce pressure loss and internal skin friction in the combustion chamber since excludes necessity to introduce different kinds of stabilizing device into the flow (strut, wedge, vortex generator). This simplifies the combustion chamber design, enables heat protection, and reduces the combustion chamber weight.

This study confirms the ignition of hydrogen occurring at a high gain in pressure and heat fluxes. In future, the efforts will be focused on studying thermal regimes for a combustion chamber at unsteady process of ignition and flame stabilization.

References

1. **K.R. Jackson, M.R. Gruber, and S. Buccellato,** Mach 6–8 hydrocarbon-fueled scramjet flight experiment: the HIFIRE flight 2 project, J. Propulsion and Power, 2015, Vol. 31, No. 1, P. 36–53.
2. **J.P. Drummond,** Methods for prediction of high-speed reacting flows in aerospace propulsion, AIAA J., 2014, Vol. 52, No 3, P. 465–485.
3. **A. Ingenito and C. Bruno,** Physics and regimes of supersonic combustion, AIAA J., 2010, Vol. 48, No 3, P. 515–525.
4. **R. Masumoto, S. Tomioka, K. Kudo, A. Murakami, K. Kato, and H. Yamasaki,** Experimental study on combustion modes in a supersonic combustor, J. Propulsion and Power, 2011, Vol. 27, No. 2, P. 346–355.
5. **D.J. Micka and J.F. Driscoll,** Stratified jet flames in a heated (1390 K) air cross-flow with auto-ignition, Combust. Flame, 2012, Vol. 159, P. 1205–1214.
6. **C. Segal,** The Scramjet Engine: Process and Characteristics, Cambridge University Press, 2009.
7. **H.M. Altay, R.L. Speth, D.E. Hudgins, and A.F. Ghoniem,** The impact of equivalence ratio oscillations on combustion dynamics in a backward-facing step combustor, Combust. Flame, 2009, Vol. 156, P. 2106–2116.

8. **W. Huang, L. Jin, L. Yan, and J. Tan,** Influence of jet-to-crossflow pressure ratio on nonreacting and reacting processes in a scramjet combustor with backward-facing steps, Inter. J. Hydrogen Energy, 2014, Vol. 39, No. 36, P. 21242–21250.
9. **A. Ben-Yakar and R. Hanson,** Cavity flame-holders for ignition and flame stabilization in scramjets: an overview, J. Propulsion and Power, 2001, Vol. 17, No. 4, P. 869–877.
10. **M.R. Gruber, J.M. Donbar, and C.D. Carter,** Mixing and combustion studies using cavity-based flameholders in a supersonic flow, J. Propulsion and Power, 2004, Vol. 20, P. 769–779.
11. **F.W. Barnes and C. Segal,** Cavity-based flameholding for chemically-reacting supersonic flows, Prog. Aerosp. Sci., 2015, Vol. 76, P. 24–41.
12. **O.R. Kummitha, L. Suneetha, and K.M. Pandey,** Numerical analysis of scramjet combustor with innovative strut and fuel injection techniques, Inter. J. Hydrogen Energy, 2017, Vol. 42, No. 15, P. 10524–10535.
13. **F. Genin and S. Menon,** Simulation of turbulent mixing behind a strut injector in supersonic flow, AIAA J., 2010, Vol. 48, No. 3, P. 526–533.
14. **K.Y. Hsu, C.D. Carter, M. Gruber, T. Barhorst, and S. Smith,** Experimental study of cavity-strut combustion in supersonic flow, J. Propulsion and Power, 2010, Vol. 26, No. 6, P. 1237–1246.
15. **V.A. Vinogradov, M.A. Goldfeld, and A.V. Starov,** Ignition and combustion of hydrogen in a channel with high supersonic flow velocities at the channel entrance, Combustion, Explosion, and Shock Waves, 2013, Vol. 49, No. 4, P. 383–391.
16. **N.C. Grady, R.W. Pitz, and C.N. Carter,** Supersonic flow over a ramped-wall cavity flame holder with an upstream strut, J. Propulsion and Power, 2012, Vol. 28, No. 5, P. 982–990.
17. **K. Kobayashi, S. Tomioka, and T. Mitani ,**Supersonic flow ignition by plasma torch and H2/O2 torch, J. Propulsion and Power, 2004, Vol. 20, No. 2, P. 294–301.
18. **A. Starikovskiy and N. Aleksandrov,** Plasma-assisted ignition and combustion, Prog. Energy Combust. Sci., 2013, Vol. 39, P. 61–110.
19. **K.V. Savelkin, D.A. Yarantsev, I.V. Adamovich, and S.B. Leonov,** Ignition and flameholding in a supersonic combustor by an electrical discharge combined with a fuel injector, Combust. Flame, 2015, Vol. 162, No. 3, P. 825–835.
20. **Q. Liu, D. Baccarella, B. McGannm, T. Lee, and H. Do,** Experimental investigation of single jet and dual jet injection in a supersonic combustor, AIAA Paper, 2018, No. 2018–1363.
21. **J.A. Schetz, L. Maddalena, R. Throckmorton, and R. Neel,** Complex wall injector array for scramjet combustors, AIAA Paper, 2008, No. 2008–0105.
22. **M.P. Golubev and M.A. Goldfeld,** Gas jet interaction with supersonic cross flow in a channel, Tech. Phys. Lett., 2018, Vol. 45, P. 1234–1237.
23. **F. Ladeinde,** A critical review of scramjet combustion simulation, AIAA Paper, 2009, No. 2009–127.
24. **R.A. Baurle and J.R. Edwards,** Hybrid Reynolds-averaged/large eddy simulations of a coaxial supersonic free jet experiment, AIAA J., 2010, Vol. 48, No. 3, P. 551–571.
25. **E.D. Gonzalez-Juez, A.R. Kerstein, S. Menon, and R. Ranjan,** An analysis of the basic assumptions of turbulent-combustion models with emphasis on high-speed flows, AIAA Paper, 2015, No. 2015–1380.
26. **M. Gamba and M.G. Mungal,** Ignition, flame structure, and near-wall burning in transverse hydrogen jets in supersonic crossflow, J. Fluid Mech., 2015, Vol. 780, P. 226–273.
27. **J. Melguizo-Gavilanes, L.R. Boeck, R. Mével, and J.E. Shepherd,** Hot surface ignition of stoichiometric hydrogen-air mixtures, Inter. J. Hydrogen Energy, 2017, Vol. 42, No. 11, P. 7393–7403.
28. **V. Moureau, C. Berat, and H. Pitsch,** An efficient semi-implicit compressible solver for large-eddy simulations, J. Comput Phys., 2007, Vol. 226, No. 2, P. 1256–1270.
29. **T. Hiejima,** Effects of streamwise vortex breakdown on supersonic combustion, Physical Review E, 2016, Vol. 93, No 4, P. 43115–43115.
30. **B. Liu, G.Q. He, F. Qin, J. An, S. Wang, and L. Shi,** Investigation of influence of detailed chemical kinetics mechanisms for hydrogen on supersonic combustion using large eddy simulation, Inter. J. Hydrogen Energy, 2019, Vol. 44, No. 10, P. 5007–5019.
31. **F. Ladeinde and W. Li,** Differential turbulent supersonic combustion of hydrogen, methane, and ethylene, without assisted ignition, AIAA J., 2018, Vol. 56, No. 12, P. 4870–4883.
32. **A.A. Maslov, V.V. Shumsky, and M.I. Yaroslavtsev,** High-enthalpy hot-shot wind tunnel with combined heating and stabilization of parameters, Thermophysics and Aeromechanics, 2013, Vol. 20, No. 5, P. 527–538.
33. **M.A. Goldfeld, Yu.V. Zakharova, A.V. Fedorov, and N.N. Fedorova,** Effect of the wave structure of the flow in a supersonic combustor on ignition and flame stabilization, Combustion, Explosion, and Shock Waves, 2018, Vol. 54, No. 6, P. 3–16.
34. **K. Mahesh,** The interaction of jets with crossflow, Annu. Rev. Fluid Mech., 2013, Vol. 45, No. 1, P. 379–407.
35. **A.S. Pusey, V. Wheatley, and R.R. Boyce,** Behavior of multiple-jet interactions in a hypersonic boundary layer, J. Propulsion and Power, 2015, Vol. 31, No. 1, P. 144–155.
36. **R.T. Milligan and T. Mathur,** Dual mode scramjet combustor: analysis of two configurations, AIAA Paper, 2010, No. 2010–0751.